Carbon 105 (2016) 377–386

Contents lists available at ScienceDirect

Carbon

journal homepage: www.elsevier.com/locate/carbon

Phonon properties in different types of single-walled carbon nanotube thin films probed by Raman spectroscopy

Anna Duzynska*, Michal Swiniarski, Anna Wroblewska, Anna Lapinska, Klaudia Zeranska, Jaroslaw Judek, Mariusz Zdrojek**

Faculty of Physics, Warsaw University of Technology, Koszykowa 75, 00-662, Warsaw, Poland

ARTICLE INFO

Article history:
Received 4 February 2016
Received in revised form
8 April 2016
Accepted 26 April 2016
Available online 27 April 2016

ABSTRACT

We report a temperature-dependent (70–450 K) Raman study of single-walled carbon nanotube (CNT) thin films as a function of their thickness and the conductivity type of the nanotubes used to fabricate these films. The CNT films Raman G mode positions and widths exhibit two apparent regimes, a nonlinear temperature dependence at low temperatures (<270 K), which is explained by the phenomenon of optical phonon decay, and a linear temperature dependence above 270 K. The first-order temperature coefficient, determined for the linear regime, depends on the film thickness and type of CNTs, changed up to 20%. In addition, we observed another factor causing phonon shifts that is not related to the temperature but strongly depend on the film thickness and conductivity type of the CNTs. Finally, we ascertained the local temperature changes of the film samples upon laser heating as a function of the global temperature, demonstrating significant differences in the heating process, suggesting that heat evacuation efficiency depends type of the film, its thickness and global temperature. These results contribute to the understanding of the thermal properties and heat dissipation in CNT films, which are crucial for use in a variety of future applications.

1. Introduction

Carbon nanotubes (CNTs), because of their unusual optoelectronic and thermal properties, are a potential candidate for a broad range of applications, *e.g.,* as supercapacitors [1], actuators [2], batteries [3], solar cells [4], and heat spreaders [5]. Advances in production methods now enable fabrication of high-quality chirality-selected individual tubes [6] and more complex systems, such as nanotube composites [7] or thin films [8], which are much more attractive for broader industrial applications. Particular attention is currently paid to CNT films, wherein nanotubes are arranged close to each other. However, interactions between tubes can affect the properties of the whole system and change its behavior compared with individual tubes. Therefore, there is an urgent need to investigate these new properties prior to any further application. One of the most important factors during the design and production of CNT film devices is heat dissipation. Thus, understanding the thermal and phonon properties of various CNT films is of great importance.

The thermal properties of individual carbon nanotubes were extensively analyzed using different measurements techniques, including the thermal coefficient of resistance [9], the 3ω [10] and the Raman shift method [11]. Researchers studied the thermal conductivity and the heat dissipation properties by taking into account the number of walls, length, diameter, chirality, vacancy and defect concentration of the carbon nanotubes [12] and various theoretical models, for example, an empirical model [9], a wave vector model [13] or ballistic-to-diffusive crossover [14]. Now, we may ask to what extent are these properties changed when the tubes are brought together into a form of a thin film? Some answers are shown in the studies on the thermal conductivity (κ) of CNT thin films [15] [16], [17], focused on the volume fraction and arrangement of CNTs inside the film [12]. Many of those reports show that significant divergences in the values of κ are found, for example, 0.1 W m^{-1} K^{-1} for unoriented networks [18], 18.3 W m^{-1} K^{-1} for suspended high-density single-walled CNT thin films [16], and 20 W m^{-1} K^{-1} for multiwalled carbon nanotube mats [19]. Moreover, recent research demonstrates temperature-dependent

* Corresponding author.
** Corresponding author.
E-mail addresses: aniaduz@if.pw.edu.pl (A. Duzynska), zdrojek@if.pw.edu.pl (M. Zdrojek).

http://dx.doi.org/10.1016/j.carbon.2016.04.064
0008-6223/

phonon behavior for individual nanotubes [20] or bundles [21] in the high temperature range (>300 K). Additionally, semiconducting single wall carbon nanotube (SWCNT) thin films have been investigated and show a non-linear temperature dependence of the phonon shifts [22]. However, to date, there have been no extensive studies that directly considered the temperature-induced phonon behavior in SWCNT films with different conductivity types (semiconducting or metallic) or in different thicknesses of those films. We propose verifying the hypothesis that different tube-tube interfaces and the number of interfaces in the film are reflected in the phonon properties. Understanding how the phonon thermal properties of various type high-density CNT thin films differ as a function of the thickness and conductivity type would be an important contribution to reveal the heat diffusion in such structures.

In this work, we demonstrate the evolution of the temperature-dependent phonon properties in various types of SWCNT thin films, probed by Raman spectroscopy. We considered thin films with different thicknesses and types of conductivity (semiconducting, metallic and mixed CNTs). We show the G band shift and the corresponding linewidth nonlinear behavior in the temperature range (70–450 K) with different laser power irradiation and explore how the local temperature of the samples changes upon laser heating. Using this approach, we demonstrate that the most efficient heat dissipation mechanism is seen for metallic films. Using statistical Raman measurements (at room temperature), an additional contribution to the phonon shift that does not depend on the temperature was observed, but this contribution is related to the film thickness and type of nanotube used. Our work contributes to the understanding of the thermal properties and heat dissipation in CNT films, which are extremely important for various future applications.

2. Experimental section

Carbon nanotube films were fabricated via a vacuum filtration method and deposited onto a Si/SiO_2 substrate. Films were prepared using a water solution of separated semiconducting, metallic and mixed SWCNTs (from NanoIntegris, Iso-Nanotubes, 99% purity) with tube diameters from 1.2 nm to 1.7 nm and lengths in the range of 0.1–4 μm. We note that in the case of mixed carbon nanotubes, films were fabricated with using a mixture of semiconducting and metallic solution of the nanotubes with the ratio of 1:1. We note that the average length distribution for all tube types is nearly the same (data from NanoIntegris). The concentration of CNTs in all solutions was 0.01 mg ml^{-1}. An appropriate amount of each solution was vacuum filtered onto the mixed cellulose ester membrane (MCE, 0.025-μm pore size, 25 mm diameter) to achieve a specified thickness of the SWCNT films, 50 nm and 200 nm for each type of nanotube. The vacuum process membranes were dried in a furnace at 70 °C for an hour and then immersed in toluene for a few minutes, which did not dissolve the filter or destroy the CNT film but allowed better adhesion between the film and the substrate. Next, a 5 × 5 mm piece of the each SWCNT film coated MCE membrane was cut and transferred face down onto the Si/SiO_2 substrate (a 285-nm-thick layer of silicon dioxide). The MCE membrane was dissolved in the vapors of acetone. Then, the samples were immersed into liquid acetone to remove the residual filter. In the end, the samples were rinsed with methanol and gently dried by the nitrogen stream. We note that this method can produce high-density films (see Fig. 1) with a uniform thickness and, also important, high purity without residual surfactants (proved by Raman, data not shown here).

In this work, we use six types of samples consisting of different types of nanotubes and different film thicknesses, labeled as S-50, S-200, M-50, M-200, SM-50 and SM-200 (see a top photograph in Fig. 1). Their designation are as follows: the letter stands for the type of nanotube used (S – semiconducting, M – metallic, and SM – mixed), and the number corresponds to the film thickness in nm. The thickness of each film has been determined by an atomic force microscope (NT-MDT).

A scanning electron microscope (SEM) was used to characterize the topography of the film surface and to illustrate the arrangement of the nanotubes. The results are shown in Fig. 1. It is easily seen that the vacuum filtered films have the same nanotube composition independent of the sample thickness and the type of CNTs used. The unoriented arrangement of nanotubes inside the film is common for all samples.

To confirm the type of nanotubes used, the absorption spectra (using a Cary 5000 spectrometer) of two semiconducting (S-50 and S-200) and two metallic (M-50 and M-200) SWCNT films on glass substrate were obtained (see Fig. 2a). The spectra for the semiconducting films exhibit three characteristic optical transition bands, S_{33}, S_{22} and S_{11}, and similarly, for the metallic films, a typical interband transition, M_{11}, is observed [23]. Moreover, according to expectations, the intensity of the peaks is correlated with the film thickness (higher intensity for a thicker film). These results clearly confirm that the nanotubes labeled as semiconducting and metallic possess such type of conductivity.

The Raman spectra were collected using a Renishaw spectrometer with a 514 nm laser excitation line (2.41 eV) in a backscattering configuration (see supplementary information for spectra taken for 633 nm laser line, for comparison), where the laser beam was focused (with objective 50×) onto the CNT film deposited on the Si/SiO_2 substrate. The focused beam's diameter on the sample was approximately 1 μm. To study the homogeneity of the thin films, micro-Raman G^+ peak maps were collected. In this analysis, we choose G^+ mode because its intensity is much higher than that of G^- or 2D. The map area for each sample was 20 × 20 μm, with a rate of 1 μm (the observed effects were also confirmed by the measurements on the other samples and the bigger scan areas).

The temperature-dependent Raman spectra of the samples were obtained using an optical cryostat (Oxford Instrument). The global temperature was changed from 70 to 450 K, with a stability of 0.1 K, under a pressure of approximately 10^{-6} mbar. Measurements were performed for two incident laser powers (P_L), 0.3 and 5.4 mW (calibrated on the sample). For the lower value of P_L, no laser-induced heating of the film was expected. In contrast, the higher value caused additional heating of the samples. In both cases, no local irreversible change in the samples' morphology was noticed upon heating and cooling. The integration time of the Raman spectra was dependent on the laser power and was the scale bars represents approximately 50 s for the lower laser power and 20 s for the higher laser power. The peak positions and their linewidth (full width at half maximum, FWHM) values were obtained through a Lorentzian fit of the Raman spectra. In this work, the temperature-dependent Raman spectra are analyzed based on the G^+ band shift.

3. Results and discussion

Fig. 2b shows the initial single-point Raman measurements of six different CNT thin films collected at room temperature, ambient pressure, and for a low incident laser power of 0.3 mW. All spectra in Fig. 2b are normalized for sake of comparison (see Supplementary information for Raman spectra without normalization).

Interestingly, in Fig. 2b all samples have similar Raman signatures, and little difference is visible between the spectra of the

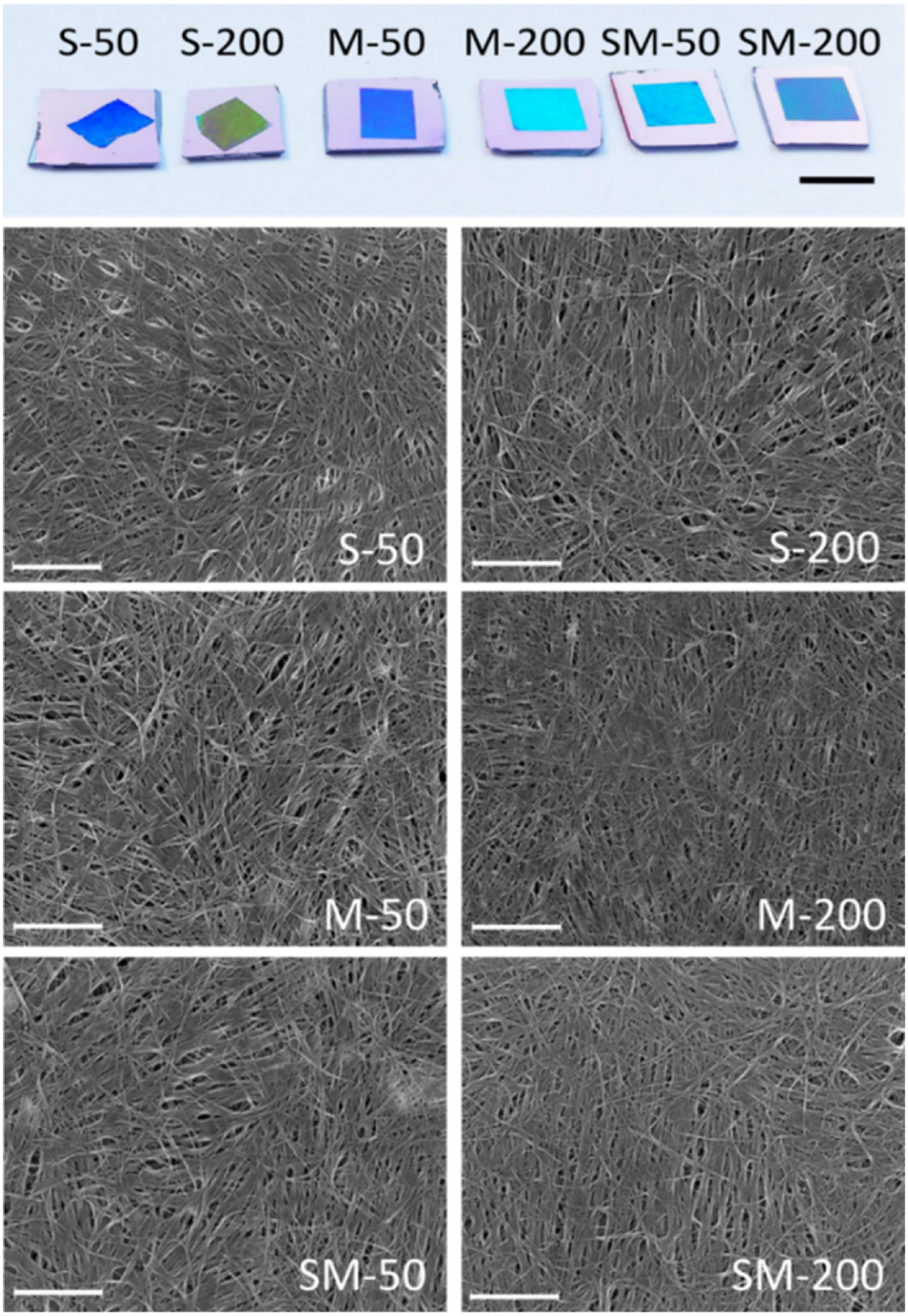

Fig. 1. (Top) Photograph of an exemplary set of the samples; the scale bar represents 6 mm. (Bottom) A set of SEM images of the analyzed SWCNT thin films; the scale bars represents 600 nm.(A color version of this figure can be viewed online.)

semiconducting and metallic CNT films (only slightly different shape and position of RBM mode). The G mode for SWCNTs consists of two main components, G^+ and G^- (see Fig. 1d), and it is known that the G^- lineshape is highly sensitive to whether the SWCNT is metallic (Breit-Wigner-Fano lineshipe) or semiconducting (Lorentzian lineshipe) [24]. In our case, the same Lorentzian lineshape of the G^- mode for all samples is likely due to the tube–tube interactions inside the thin film, where neighboring tubes are tightly arranged [25,26] and/or the resonance conditions for the semiconducting nanotubes for 514 nm laser line. In Fig. 2b the lineshape of the G^+ band is Lorentzian, as expected, but slight changes in the peak position, depending on the type of tubes, have been detected (this effect is explained later in the statistical analysis of the Raman spectra). We note that for 633 nm laser line Raman spectra are different (see Supplementary information). For example, the BWF lineshipe of the G^- mode for metallic carbon nanotube thin films is clearly observed. However, signals from the G^- and G^+ mode for this laser line are highly complex and difficult

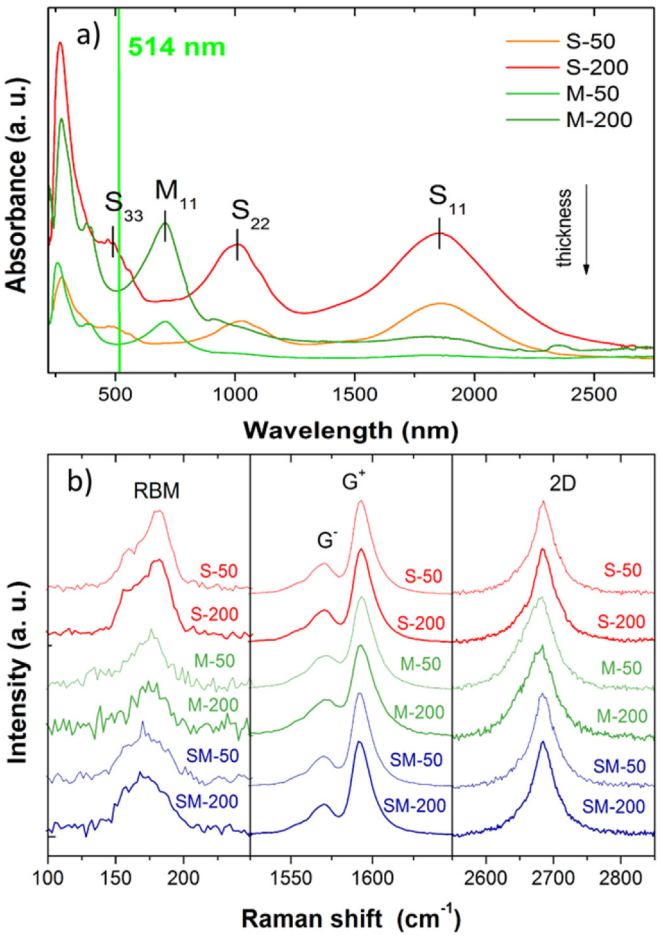

Fig. 2. (a) The absorbance spectra of the S-50, S-200, M-50 and M-200 carbon nanotube films on the glass substrate. The number in the sample name stands for the film thickness in nm. The vertical green line indicates the 514 nm laser line used in this work. The absorption coefficients for this line are 0.18 and 0.57 for S-50 and S-200 respectively; 0.1 and 0.39 for M-50 and M-200, respectively. (b) Normalized Raman spectra for all SWCNT films (on SiO_2/Si substrate) taken at ambient conditions, with a low incident laser power of 0.3 mW.(A color version of this figure can be viewed online.)

to fit, so for further analysis in our work, the 514 nm laser line is used. On the other hand, the optical absorption spectra of these films exhibit significant and typical differences between the semiconducting and metallic nanotubes, showing signatures of interband optical transition.

To assess the thermal properties of the phonons in different CNT films, we look at the Raman G band for a wide range of temperatures. An example of normalized Raman spectra for the metallic thin film of CNTs measured at selected temperatures is shown in Fig. 3a. Detailed temperature-dependent Raman shifts of the G^+ mode for all CNT films are shown in Fig. 3b. Data were collected for the 70–450 K temperature range using 0.3 mW of incident laser power (where no laser-induced heating is expected). As can be seen for each sample, the peak position is downshifted as the temperature increases and clearly exhibiting two regimes. The position of the G modes tends to saturate at the lower temperature range, below 270 K, and at the higher temperature range (≥270 K). Increasing the temperature causes a linear blue shift of the Raman modes' position. We note that for the observed temperature-dependent phonon shifts, only the thermal effects $(\partial\omega/\partial T)_V$ were responsible because the volume of the related lattice expansion effect is on the order of 10^{-5} 1/K and can be neglected during further analyses [27].

To describe the phonon behavior in details, we used two approaches: the commonly used linear approximation and the nonlinear approximation based on Balkanski theory [28].

In the first approach, to soften the G^+ mode for a higher temperature range, we used a linear approximation with a formula [29]:

$$\omega(T) = \omega_0 + \chi_T T \tag{1}$$

where ω_0 is the approximation of the phonon frequency at zero temperature, and χ_T is the first-order temperature coefficient. The function was fitted to the data at a temperature range from 270 to 450 K. The obtained χ_T of the samples oscillate around the value of -0.02 cm^{-1}/K. However, the main trend shows a lower thermal coefficient for the films, which include metallic nanotubes (*e.g.*, 0.0188 cm^{-1}/K for M-200 and -0.0191 cm^{-1}/K for SM-50). Importantly, the χ_T change as a function of the film thickness for each type of nanotube (in the case without laser heating) is non-significant and equals 1%, 14% and 5% for the semiconducting, metallic and mixed CNT films, respectively. Therefore, depending on the film thickness and type of CNT, the first-order temperature coefficient can change up to 20%. The fitted slopes for all the samples are shown in Table 1 compared with other carbon materials. The temperature coefficients for our SWCNT films are similar to those measured for DWCNT [30] or MWCNTs [31] and are slightly higher than for supported graphene [29].

A second approach, used to characterize the change of the Raman G^+ peak position as a function of the temperature, is related to the effect of the optical phonon decay of two acoustic phonons (three phonon process) with equal energies due to lattice potential anharmonicity [28]:

$$\omega(T) = \omega_0 + A\left(1 + \frac{2}{e^x - 1}\right) \tag{2}$$

where $x = \hbar(\omega_0/2)/k_B T$, ω_0 is the phonon frequency at T = 0 K, $\hbar$ is Planck's constant, k_B is the Boltzmann constant, A is the fitting parameter, and T is the sample temperature without laser heating ($P_L = 0.3$ mW). This approach is represented by the solid lines in Figs. 3 and 5b. The fitted parameters ω_0 and A are included in Table 1. We notice that this model better fits the experimental data of the $\omega(T)$ than the first approach, especially in the range of the lower temperatures (<270 K). Similar nonlinear behavior was observed for supported SWCNTs (where this effect was related to contributions from electron-phonon interactions) [21], semiconducting SWCNT thin films [22] and also for two dimensional materials, such as MoS_2 [33].

At higher temperatures, when we take into consideration only the first-order Taylor expansion, eq. (2) converge to a linear dependence in Eq. (1) because: $\omega(T) \xrightarrow{x=\hbar\omega_0/2k_BT \ll 1} \omega_0 + A + \frac{4Ak_B}{\hbar\omega_0}T = \omega_0' + \chi_B T$, where $\omega_0' = \omega_0 + A$, and $\chi_B = 4Ak_B/\hbar\omega_0$.

Fig. 3c shows the temperature dependence of the G^+ Raman peak width at half maximum (FWHM) for all samples (data are presented for a lower laser power, where laser heating is not expected). For all Raman characteristics, the increase of the linewidth with increasing temperature is clearly pronounced for temperatures above 270 K and tends to saturate for lower temperatures (T < 270 K). The measured data were adapted as a function of the three-phonon process with the following equation [28]:

$$\Gamma(T) = \Gamma_0\left(1 + \frac{2}{e^x - 1}\right) \tag{3}$$

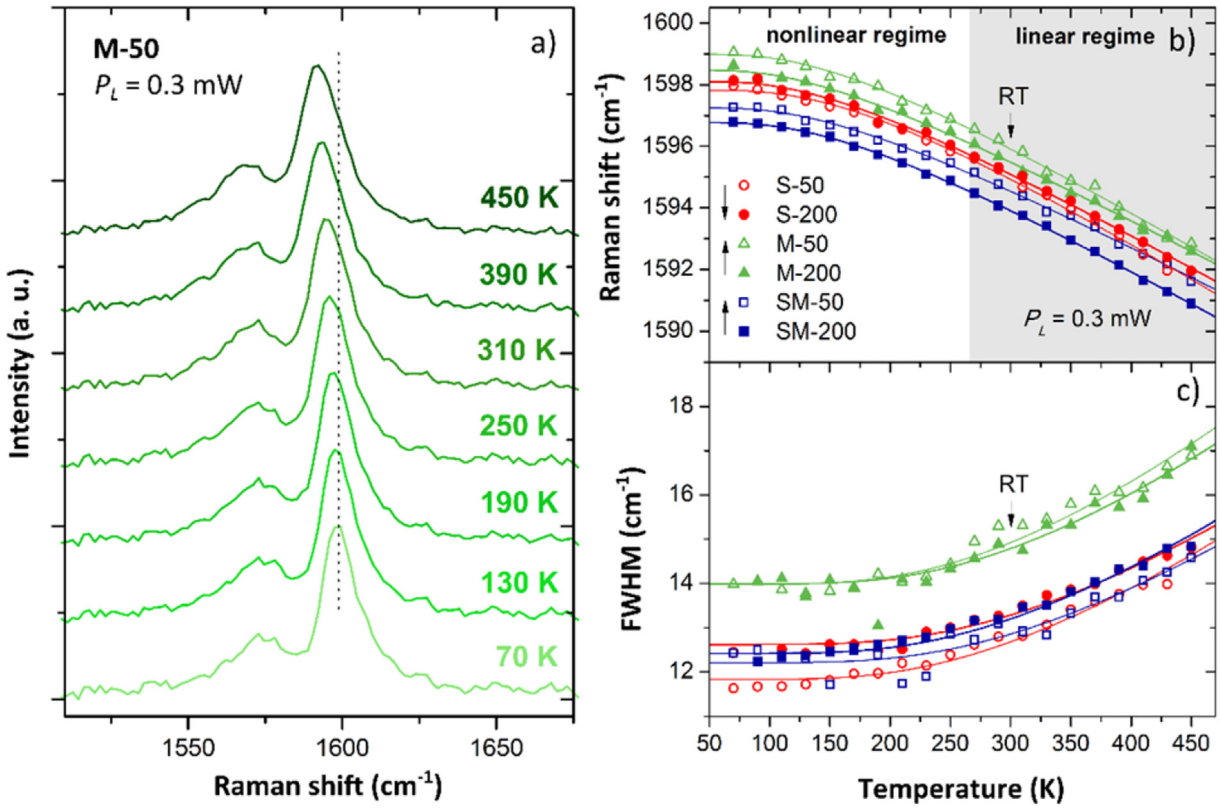

Fig. 3. (a) Normalized Raman spectra for 50 nm thick film made of metallic tubes, shown at selected temperatures in the range of 70–350 K. (b) Comparison of the temperature dependence of the Raman G^+ peak position (curves represent fit to Eq. (2)). The arrows demonstrate the direction of the phonon shift for different thicknesses. (c) FWHM of the G^+ mode (curves represent fit to Eq. (3)) for the SWCNT thin films. Data were collected with a low laser power, $P_L = 0.3$ mW. RT stands for room temperature.(A color version of this figure can be viewed online.)

Table 1
Calculated parameters from Eqs. (1)–(3). Data taken at 0.3 mW laser power. Eq. (1) fitted in the 270–450 K range and Eqs. (2) and (3) fitted in the 70–450 K range.

Sample	χ_T (cm^{-1}/K) Eq. (1)	ω_0 (cm^{-1}) Eq. (1)	ω_0 (cm^{-1}) Eq. (2)	A (cm^{-1}) Eq. (2)	Γ_0 (cm^{-1}) Eq. (3)
S-50	−0.0228	1601.9	1604.3	−6.46	11.83
S-200	−0.0208	1601.4	1603.1	−5.00	12.62
M-50	−0.0219	1602.6	1604.4	−5.41	13.99
M-200	−0.0188	1601.1	1602.9	−4.38	13.99
SM-50	−0.0191	1600.3	1602.0	−4.77	12.21
SM-200	−0.0202	1600.0	1602.2	−5.38	12.42
SWCNT + catalysts [32]	−0.0189	1599.1	–	–	–
DWCNT [30]	−0.022	–	–	–	–
MWCNT [31]	−0.023	–	–	–	–
Supported graphene [29]	−0.016	1584.0	–	–	–

where Γ_0 is the peak width at zero temperature. The fit parameter for each sample is presented in Table 1. The theoretical model describes the experimental data well, which confirms that the nonlinear behavior of Γ as a function of the temperature is related to the phonon decay process.

Comparing the frequency shift as a function of temperature $\omega(T)$ for each sample (in Fig. 3b) yields interesting results. Note that the general course of the G^+ Raman peak position as a function of the temperature is similar for all types of SWCNTs and exhibits a similar nonlinear tendency. However, for films that include metallic tubes, the $\omega(T)$ functions are shifted toward lower energies for the thicker films (see green and blue data points in Fig. 3b in the web version). For pure semiconducting films, the situation is reversed, and the $\omega(T)$ function for the thicker film is, in general, upshifted with respect to the 50 nm thick sample (see red data points in Fig. 3b in the web version). Moreover, there is a significant difference in the $\omega(T)$ plots for different types of films (M, S or SM). Thus, it seems that the phonons in the CNT films are shifted because of the temperature, but the shift also depends on their thickness and the type of CNT.

To extract the factors (other than temperature) that cause phonon shifts, we employ a statistical analysis of the G^+ phonon at room temperature, for which spatially resolved Raman maps have been used (see experimental section for details). The obtained results for the G^+ peak position and its width at half maximum (FWHM) are presented as histograms in Fig. 4 (each histogram contains data from approximately 450 spectra). The first striking feature is that the average of the G^+ peak position (from a Gaussian fit) depends on the film thickness, and it is also different for each type of nanotube. Interestingly, for the CNT films, which include metallic nanotubes, the G^+ peak position for the thicker film is shifted toward the lower energies compared with the 50 nm film

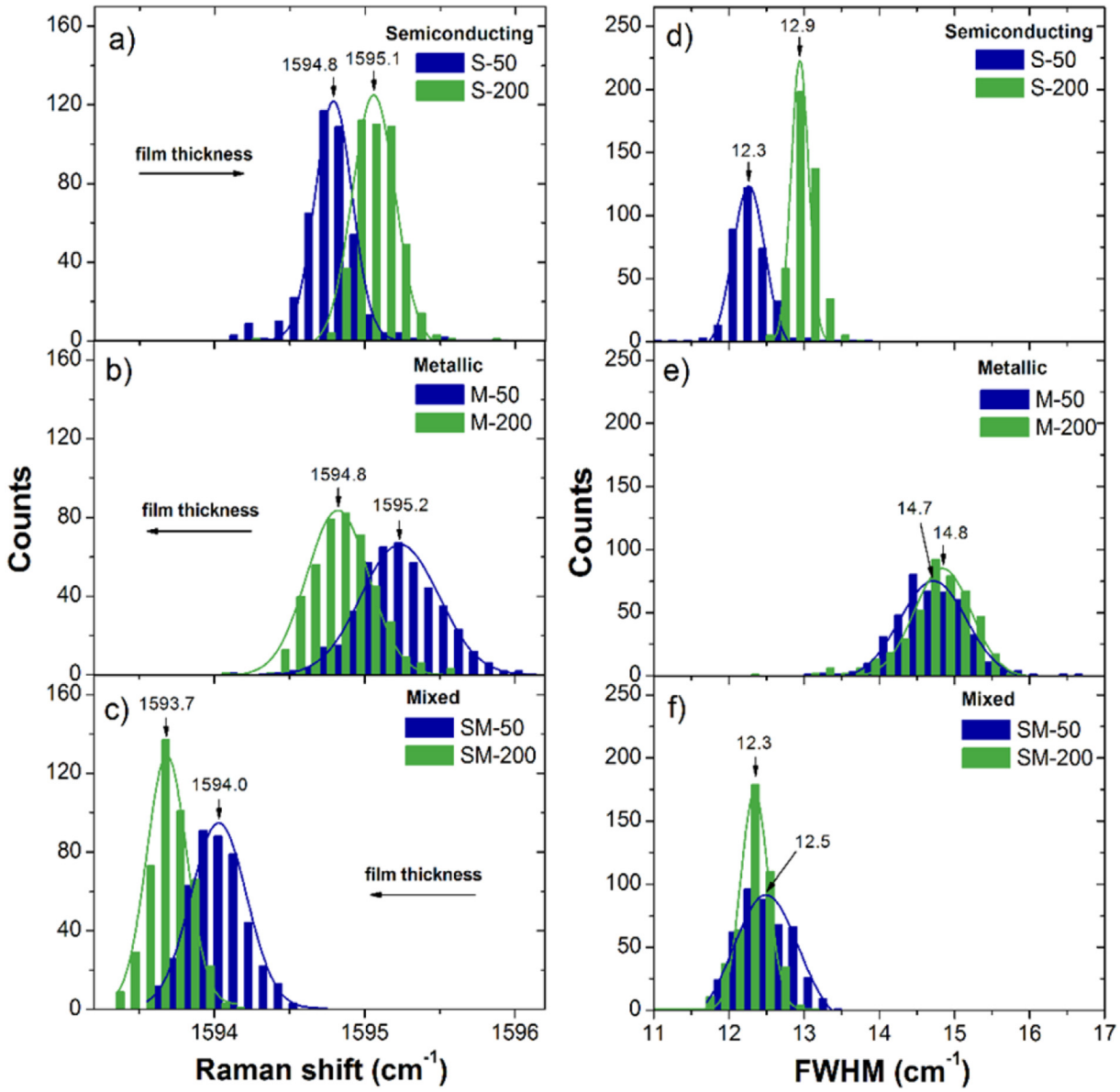

Fig. 4. Histograms of the Raman G^+ peak position for semiconducting (a), metallic (b), and mixed (c) SWCNT thin films, and the FWHM of the G^+ mode for semiconducting (d), metallic (e), and mixed (f) carbon nanotube films; the results for the thinner films (50 nm) are represented by blue and for the thicker films (200 nm) by green. The curves represent the fit of the Gaussian function.(A color version of this figure can be viewed online.)

made of semiconducting tubes (see horizontal arrows in Fig. 4). For the semiconducting thin film, the situation is reversed, and the position of G^+ is shifted towards the lower energies for the thinner film. For the film with mixed metallic and semiconducting tubes, an additional downshift of G^+ is seen compared with the single-type films. Another interesting feature is related to the FWHM of the investigated peak. In particular, for the films containing metallic tubes, the FWHM is nearly independent of its thickness, whereas for semiconducting films, a broadening of the peak is observed for thicker films. In addition, the width of the G band for metallic film is noticeably broader compared with the rest of the film types. Importantly, all these results are in good agreement with the temperature-dependent measurements (see Fig. 3b and c at room temperature), showing that the Raman shifts and peak width are also tube-type and thickness dependent.

These behaviors may be explained by the interplay of several effects, including nanotube doping, stress and the optical absorption of the nanotubes. The first one is related to the high sensitivity of frequency ω_{G^+} (peak position) to the charge transfer from external dopants [34–38]. One can expect upshifts of ω_{G^+} for acceptors and downshifts for donors [24]. Thus, it is possible that the tube–tube interaction in the film may promote charge transfer in the entire network, causing a Raman peak shift. For example, as seen in Fig. 4b, the metallic nanotubes serve as an donor medium, causing a downshift of the peak position with increasing thickness (larger volume of the CNT film is measured). Second, the stress in nanotubes that might originate from the sample fabrication process (vacuum filtration) or just from tube bundling could influence the measured peak position or its width [39,40]. However, we find the stress in the film induced by the fabrication process rather unlikely because many different samples give fully reproducible results. Finally, the optical absorption that is different (due to thickness and type of tubes) for all investigated films (see Fig. 2a) may also influence the peak position, for instance, by increasing the absorbed

laser power for the semiconducting film, thus increasing the local temperature.

Resolving all the above effects that may be responsible for the phonon energy and life time (peak width) change seen at room temperature in different CNT films (Fig. 4) requires further study and may be a starting point for future work.

Now, we turn our attention to the laser-induced temperature effects. In particular, we determine how the laser power affects the local temperature of different CNT films. To see this, we measured two Raman spectra at every temperature for two laser powers (P_L), 0.3 mW and 5.4 mW (see Fig. 5). For a lower P_L value, the data and fits correspond to the data shown in Fig. 3b, where no significant heating upon laser irradiation is expected. At the higher laser power, the Raman peaks downshift because of the local heating (see full circles in Fig. 5). The difference of each peak position for all films for both laser powers ($\Delta\omega$) as a function of temperature are presented in the bottom of each graph in Fig. 5 (with the calculated slope of the fitted line). This difference corresponds to the peak position shift caused by the local heating induced only by the absorbed laser power. Therefore, this parameter can be used as a thermometer of the averaged local lattice temperature as a function of the global temperature. The negative value of the $\Delta\omega$ parameter represents the phonon downshift with increasing temperature. Interestingly, $\Delta\omega$ is a linear function of the temperature and does not follow the nonlinear behavior seen for the G peak position.

The temperature rise ΔT due to the laser power increase was at first calculated using only phonon shifts as local thermometer. We transformed Eq. (2) to receive the temperature changes as a function of the frequency shift:

$$T(\omega) = C \cdot \left[ln\left(\frac{\omega - \omega_0 + A}{\omega - \omega_0 - A}\right)\right]^{-1} \quad (4)$$

where $C = \hbar(\omega_0/2)/k_B$ and ω is the measured G^+ peak position. First, we inserted the equation data of the G^+ peak position for the lower laser power. Second, using the higher laser power, the sample temperatures without and with laser heating were obtained. The difference between the temperature of the sample for the lower and higher laser powers corresponds to the local temperature change upon laser heating. These results, as a function of the global temperature, are presented in Fig. 6 for each sample. Importantly, significantly different trends are observed depending on the type and thickness of the film. In general, for the films that contain semiconducting nanotubes, the local temperature changes nonlinearly (see the circle and square data points in Fig. 6), exhibiting a minimum at approximately 200 K. The minimum value indicated that the heat dissipation in these films is most efficient at 200 K, and it is significantly decreased for temperatures below 150 K. In the higher temperature regime, the local heating rate is also slightly increasing, but for mixed CNT films, this effect is lower (see blue lines). We note that the increase of the local temperature for the pure thin (50 nm) semiconducting film is in good agreement with our previous work [22], where we have shown a linear increase of the local heating in the temperature range 300–450 K. For metallic films, the temperature-dependent local heating linearly increases with global temperature in the entire measured range and, at the same time, is lower (for temperature <200 K) than that of the semiconducting film. The difference between the types of nanotubes is most striking for the low temperature range. Thus, the data shown in Fig. 6 suggest that films containing metallic tubes evacuate heat in a more efficient way. In addition, we noticed an interesting feature concerning the thin metallic film, namely, the local temperature change (upon laser heating) becomes negative below 200 K. There is no physical meaning behind the negative value of the local temperature change, which can go only down to zero but not below. The negative values comes from the uncertainty of determination of the peak position for given temperature (which is < 0.2 cm^{-1}). The local temperature change is determined as a difference between two Raman shift plots (for the two laser powers) and for low temperature it is very small. Taking into account that χ for metallic tubes is -0.021 cm^{-1}/K the error bar for determination local temperature change is around $\pm$10 K. Thus, the plot can go below zero still being within the experimental error but the real temperature change is close to zero. This means that the laser is no longer heating the film with the given power density we used in the experiment.

In order to have better insight into local temperatures changes we take into account the real absorbed power for metallic and semiconducting films. For this purpose we normalized the ΔT by the optical absorption coefficient (α) for 514 nm wave length (taken from Fig. 2a) and by the laser power difference ($\Delta P_L = 5.1$ mW). The plots of $\Delta T/\alpha\Delta P_L$ are shown in Fig. 6b and are slightly different as compared to Fig. 6a. First, the slope of temperature change of thin metallic film is significantly changed for higher temperature range. Second, much more pronounced difference for heating efficiency is seen for thick and thin semiconducting film.

Possibly, all these effects stem from the different thermal conductivity of the metallic and semiconducting films, causing differences in efficiency of heat dissipation. This is likely because, from the literature, it is known that the thermal conductivity (κ) may differ between different films [17,41], thus causing a different heating effect upon laser irradiation [42,43], which implies different phonon shifts. Another, factor that can play role in the phonon shifts and heat dissipation process is the length of the tubes in various films. However, in our case the average length distribution for all types of the tubes is nearly the same, so this factor should be negligible in our consideration.

4. Conclusion

A temperature-dependent Raman analysis has been employed to show phonon behavior in different SWCNT thin films. Semiconducting, metallic and mixed carbon nanotubes have been used to fabricate films with two –thicknesses: 50 nm and 200 nm. The Raman studies were performed at temperatures from 70 K to 450 K and show the softening of the main Raman mode position (G^+) with increasing temperature. In particular, the phonon shifts in the G^+ mode exhibit a nonlinear dependence, with saturation below 270 K due to the optical phonon decay in the CNTs. Above this temperature, the temperature dependence is linear, and the calculated thermal coefficients for the SWCNT thin films oscillated around -0.02 cm^{-1}/K. However, the thermal coefficients changed by 20% depending on the type and thickness of the film. Further, we noted additional factors causing phonon shifts that are not only related to the temperature but also to the thickness of the films and the conductivity type of the CNTs. Using the temperature dependency of the phonons, we derived the local temperature changes of the film samples upon laser heating as a function of the global temperature, demonstrating significant differences in the heating process for the different thickness and types of the films, suggesting that the heat is evacuated in a more efficient way for the metallic films for low temperature and for the thicker semiconducting film as compared to the thinner one for full range of the temperature. These results contribute to the understanding of the thermal properties and heat dissipation in CNT films and note issues that demand further study. One example is determining the thermal conductivity and interfacial contact conductance for different types of SWCNT thin films as a function of the temperature. In this case, it is extremely important to develop a precise

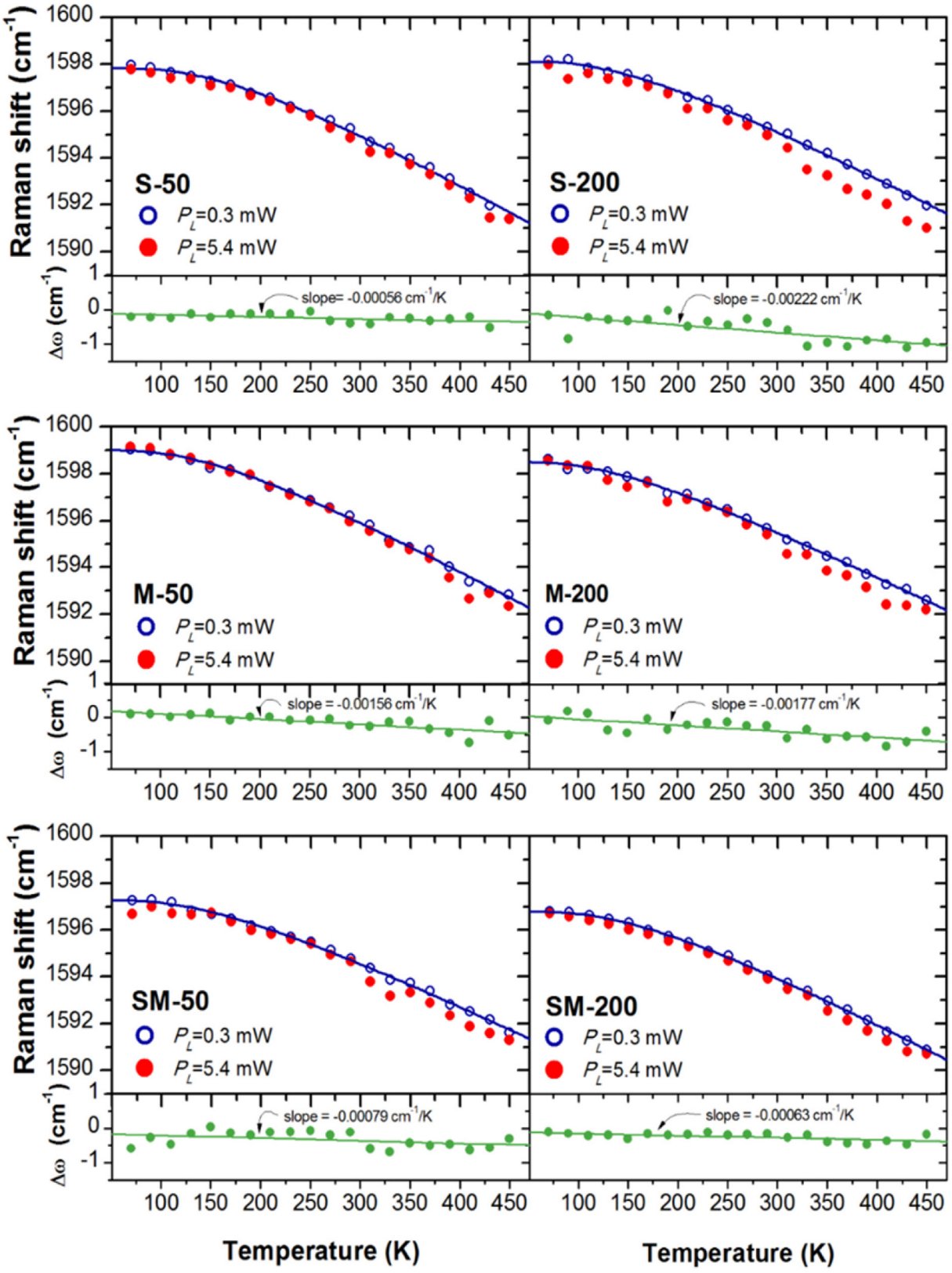

Fig. 5. Temperature dependence of the Raman peak positions in the G^+ mode for all SWCNT thin film using two laser powers, $P_L = 0.3$ mW (blue open dots) and $P_L = 5.4$ mW (red dots). The solid lines represent the fit to Eq. (2). The average uncertainty of the determination of the peak position was <0.2 cm^{-1} (error bars not shown for the sake of clarity). The lower part of each figure represents a change in the G^+ peak position due to the absorbed laser power ($\Delta\omega$) as a function of the temperature with the calculated slope of the linear fit.(A color version of this figure can be viewed online.)

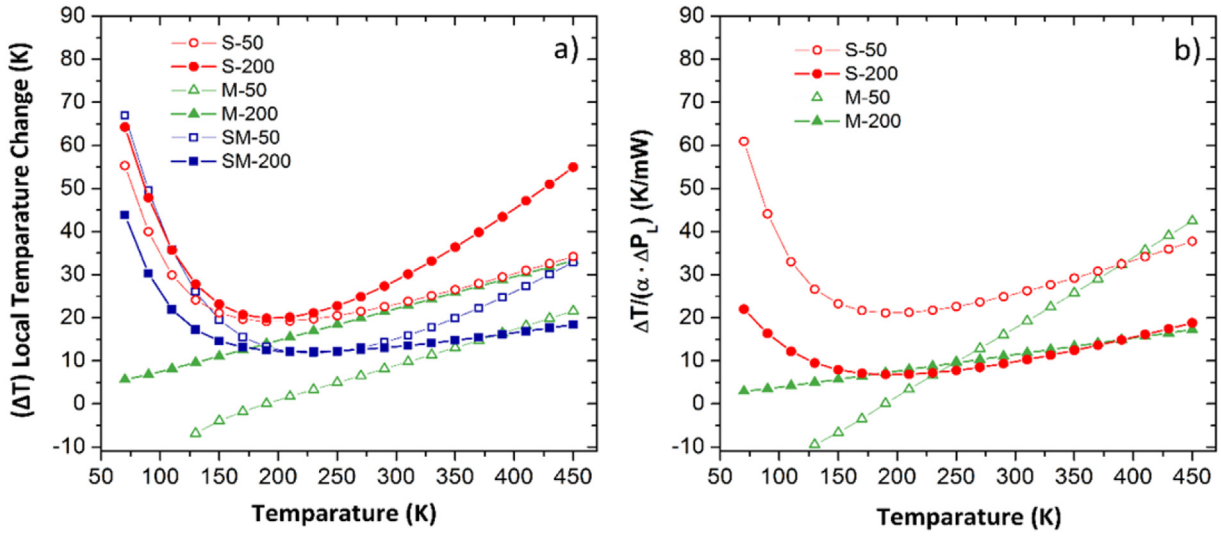

Fig. 6. (a) Calculated local temperature change (ΔT) for all samples with respect to the temperature of the environment (global) derived only from the Raman shifts (upon laser heating). The curves are only a guide for the eye. The negative value of ΔT for metallic tubes has no physical meaning and comes from the uncertainty of determination of the very small shift upon heating (see Fig. 5 for low temperature). The local temperature error bar is 10 K. (b) Local temperature change taking into account the absorption coefficient (α) for each CNT film and constant difference of laser power $\Delta P_L = 5.1$ mW.(A color version of this figure can be viewed online.)

model of the heat diffusion between neighboring nanotubes inside the film.

Notes

The authors declare no competing financial interest.

Acknowledgment

The authors thank K. P. Korona for the absorption spectra of the SWCNT films. This work was supported by the Preludium project funded by the National Science Centre (2014/13/N/ST5/01255). MZ acknowledges support from the project Lider/11/22/L-2/10/NCBR/2011.

Appendix A. Supplementary data

Supplementary data related to this article can be found at http://dx.doi.org/10.1016/j.carbon.2016.04.064.

References

[1] M. Kaempgen, C.K. Chan, J. Ma, Y. Cui, G. Gruner, Printable thin film supercapacitors using single-walled carbon nanotubes, Nano Lett. 9 (2009) 1872–1876.
[2] R.H. Baughman, C. Cui, A.A. Zakhidov, Z. Iqbal, J.N. Barisci, G.M. Spinks, et al., Carbon nanotube actuators, Science 284 (1999) 1340–1344.
[3] B.J. Landi, M.J. Ganter, C.D. Cress, R.A. DiLeo, R.P. Raffaelle, Carbon nanotubes for lithium batteries, Energy Environ. Sci. 2 (2009) 549–712.
[4] M.W. Rowell, M.A. Topinka, M.D. McGehee, H.-J. Prall, G. Dennler, N.S. Sariciftci, et al., Organic solar cells with carbon nanotube network electrodes, Appl. Phys. Lett. 88 (2006), 233506-3.
[5] K.H. Baloch, N. Voskanian, J. Cumings, Controlling the thermal contact resistance of a carbon nanotube heat spreader, Appl. Phys. Lett. 97 (2010), 063105-3.
[6] N. Komatsu, F. Wang, A comprehensive review on separation methods and techniques for single-walled carbon nanotubes, Materials 3 (2010) 3818–3844.
[7] Z. Spitalsky, D. Tasis, K. Papagelis, C. Galiotis, Carbon nanotube-polymer composites: chemistry, processing, mechanical and electrical properties, Prog. Polym. Sci. 35 (2010) 357–401.
[8] Z. Wu, Z. Chen, X. Du, J.M. Logan, J. Sippel, M. Nikolou, et al., Transparent, conductive carbon nanotube films, Science 305 (2004) 1273–1276.
[9] E. Pop, D. Mann, Q. Wang, K. Goodson, H. Dai, Thermal conductance of an individual single-wall carbon nanotube above room temperature, Nano Lett. 6 (2006) 96–100.
[10] T.-Y. Choi, D. Poulikakos, J. Tharian, U. Sennhauser, Measurement of the thermal conductivity of individual carbon nanotubes by the four-point three-ω method, Nano Lett. 6 (2006) 1589–1593.
[11] Q. Li, C. Liu, X. Wang, S. Fan, Measuring the thermal conductivity of individual carbon nanotubes by the Raman shift method, Nanotechnology 20 (2009) 145702–145705.
[12] A.M. Marconnet, M.A. Panzer, E. Goodson, Thermal conduction phenomena in carbon nanotubes and related nanostructured materials, Rev. Mod. Phys. 85 (2013) 1295–1326.
[13] Z. Wang, D. Tang, X. Zheng, W. Zhang, Y. Zhu, Length-dependent thermal conductivity of single-wall carbon nanotubes: prediction and measurements, Nanotechnology 18 (2007), 475714–4.
[14] J. Wang, J.-S. Wang, Carbon nanotube transport: ballistic to diffusive, Appl. Phys. Lett. 88 (2006), 111909-3.
[15] D. Kim, L. Zhu, C.-S. Han, J.-H. Kim, S. Baik, Raman characterization of thermal conduction in transparent carbon nanotube films, Langmuir 27 (2011) 14532–14538.
[16] S. Sahoo, V.R. Chitturi, R. Agarwal, J.-W. Jiang, R.S. Katiyar, Thermal conductivity of freestanding single wall carbon nanotube sheet by Raman spectroscopy, ACS Appl. Mater Interfaces 6 (2014) 19958–19965.
[17] A. Duzynska, A. Taube, K.P. Korona, J. Judek, M. Zrojek, Temperature-dependent thermal properties of single walled carbon nanotube thin films, Appl. Phys. Lett. 106 (2015), 183108-5.
[18] R.S. Prasher, X.J. Hu, Y. Chalopin, N. Mingo, K. Lofgreen, S. Volz, et al., Turning carbon nanotubes from exceptional heat conductors into insulators, Phys. Rev. Lett. 102 (2009) 105901–105904.
[19] Y.J. Heo, C.H. Yun, W.N. Kim, H.S. Lee, The effect of mesoscopic shape on thermal properties of multi-walled carbon nanotube mats, Curr. Appl. Phys. 11 (2011) 1144–1148.
[20] X. Zhang, F. Yang, D. Zhao, L. Cai, P. Luan, Q. Zhang, et al., Temperature dependent Raman spectra of isolated suspended single-walled carbon nanotubes, Nanoscale 6 (2014) 3949–3953.
[21] S. Chiashi, Y. Murakami, Y. Miyauchi, S. Maruyama, Temperature dependence of Raman scattering from single-walled carbon nanotubes: undefined radial breathing mode peaks at high temperatures, Jpn. J. Appl. Phys. 47 (2008) 2010–2015.
[22] A. Duzynska, J. Judek, M. Zdrojek, Temperature-dependent nonlinear phonon behavior in high-density carbon nanotube thin films, Appl. Phys. Lett. 105 (2014), 213105–5.
[23] X. Liu, T. Pichler, M. Knupfer, M.S. Golden, J. Fink, H. Kataura, et al., Detailed analysis of the mean diameter and diameter distribution of single wall carbon nanotubes from their optical response, Phys. Rev. B 66 (2002) 045411–045418.
[24] M.S. Dresselhaus, G. Dresselhaus, R. Saito, A. Jorio, Raman spectroscopy of carbon nanotubes, Phys. Rep. 409 (2005) 47–99.
[25] http://www.nanointegris.com/en/downloads.
[26] M. Baibarac, I. Baltog, A. Matea, L. Mihut, S. Lefrant, Anti-Stokes Raman spectroscopy as a method to identify the metallic and semiconducting configurations of double-walled carbon nanotubes, J. Raman Spectrosc. 46 (2015) 32–38.
[27] Y. Maniwa, R. Fujiwara, H. Kira, H. Tou, H. Kataura, S. Suzuki, et al., Thermal

expansion of single-walled carbon nanotube (SWCNT) bundles: X-ray diffraction studies, Phys. Rev. B 64 (2001), 241402(R)-3.
[28] M. Balkanski, R.F. Wallis, E. Haro, Anharmonic effects in light scattering due to optical phonons in silicon, Phys. Rev. B 28 (1983) 1928–1934.
[29] I. Calizo, A.A. Balandin, W. Bao, F. Miao, C.N. Lau, Temperature dependence of the Raman spectra of graphene and graphene multilayers, Nano Lett. 7 (2007) 2645–2649.
[30] A. Bassil, P. Puech, L. Tubery, W. Bacsa, E. Flahaut, Controlled laser heating of carbon nanotubes, Appl. Phys. Lett. 88 (2006), 173113–3.
[31] F. Huang, K.T. Yue, P. Tan, S.-L. Zhang, Z. Shi, X. Zhou, et al., Temperature dependence of the Raman spectra of carbon nanotubes, J. Appl. Phys. 84 (1998) 4022–4024.
[32] N.R. Raravikar, P. Keblinski, A.M. Rao, M.S. Dresselhaus, L.S. Schadler, P.M. Ajayan, Temperature dependence of radial breathing mode Raman frequency of single-walled carbon nanotubes, Phys. Rev. B 66 (2002) 235424–235429.
[33] A. Taube, J. Judek, C. Jastrzębski, A. Duzynska, K. Świtkowski, M. Zdrojek, Temperature-dependent nonlinear phonon shifts in a supported MoS_2 monolayer, ACS Appl. Mater Interfaces 6 (2014) 8959–8963.
[34] A.M. Rao, P.C. Eklund, S. Bandow, A. Thess, R.E. Smalley, Evidence for charge transfer in doped carbon nanotube bundles from Raman scattering, Nature 388 (1997) 257–259.
[35] H. Farhat, H. Son, G.G. Samsonidze, S. Reich, M.S. Dresselhaus, J. Kong, Phonon Softening in individual metallic carbon nanotubes due to the Kohn anomaly, Phys. Rev. Lett. 99 (2007), 145506-4.
[36] I.O. Maciel, N. Anderson, A. Pimenta, A. Hartschuh, H. Qian, M. Terrones, et al., Electron and phonon renormalization near charged defects in carbon nanotubes, Nat. Mat. 7 (2008) 878–883.
[37] W. Zhou, J. Vavro, N.M. Nemes, J.E. Fischer, F. Borondics, K. Kamaras, et al., Charge transfer and Fermi level shift in p-doped single-walled carbon nanotubes, Phys. Rev. B 71 (2005) 205423–205427.
[38] M. Stoll, P.M. Rafailov, W. Frenzel, C. Thomsen, Electrochemical and Raman measurements on single-walled carbon nanotubes, Chem. Phys. Lett. 375 (2003) 625–631.
[39] C. Thomsen, S. Reich, A.R. Goni, H. Jantoljak, P.M. Rafailov, I. Loa, et al., Intermolecular interaction in carbon nanotube ropes, Phys. Stat. Sol. B 215 (1999) 435–441.
[40] T. Yano, Y. Inouye, S. Kawata, Nanoscale uniaxial pressure effect of a carbon nanotube bundle on tip-enhanced near-field Raman spectra, Nano Lett. 6 (2006) 1269–1273.
[41] D. Kim, L. Zhu, C. Han, J. Kim, S. Baik, Raman characterization of thermal conduction in transparent carbon nanotube films, Langmuir 27 (2011) 14532–14538.
[42] J. Judek, C. Jastrzebski, A. Malolepszy, M. Mazurkiewicz, L. Stobinski, M. Zdrojek, Laser induced temperature effects in multi-walled carbon nanotubes probed by Raman spectroscopy, Phys. Stat. Sol. A 209 (2012) 313–316.
[43] I.-K. Hsu, R. Kumar, A. Bushmaker, S.B. Cronin, M.T. Pettes, L. Shi, et al., Optical measurement of thermal transport in suspended carbon nanotubes, Appl. Phys. Lett. 92 (2008), 063119-3.